Heliyon 9 (2023) e20948

Contents lists available at ScienceDirect

Heliyon

journal homepage: www.cell.com/heliyon

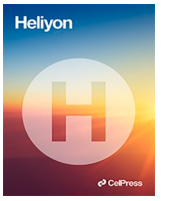

Morphological evaluation and boosted photocatalytic activity of N-doped ZnO nanoparticles prepared via Co-precipitation method

Sudipta Mondal [a,b], Sikder Ashikuzzaman Ayon [a,c], Md Saiful Islam [d], Md Shahjalal Rana [d], Md Muktadir Billah [a,*]

[a] Department of Materials and Metallurgical Engineering, Bangladesh University of Engineering and Technology, Dhaka, Bangladesh
[b] School of Materials Engineering, Purdue University, West Lafayette, IN, 47907, USA
[c] Department of Materials Science and Engineering, Northwestern University, Evanston, IL, 60208, USA
[d] Department of Nanomaterials and Ceramic Engineering, Bangladesh University of Engineering and Technology, Dhaka, Bangladesh

ARTICLE INFO

Keywords:
Co-precipitation
Nanorods
Bandgap
Photocatalysis
Recombination

ABSTRACT

Pristine and nitrogen (N) doped zinc oxide (ZnN_xO_{1-x}, x = 0, 0.005, 0.01, and 0.02) nanoparticles (NPs) were successfully synthesized using chemical co-precipitation approach. The formation of pure crystalline wurtzite ZnO phase without any second phase during N-doping was confirmed by X-ray diffraction (XRD) analysis of N-doped ZnO samples. X-ray photoelectron spectroscopic (XPS) analysis ensured the effective inclusion of nitrogen into ZnO matrix. The morphological analysis revealed the formation of nanorods as a result of N-doping. The optical band gap calculated from UV–vis spectroscopy was observed to decrease up to 1 mol.% N doping followed by a subtle increase. Photoluminescence (PL) spectra revealed that electron-hole recombination was the least for 1 mol.% N doped ZnO NPs. $ZnN_{0.01}O_{0.99}$ NPs showed superior photocatalytic activity among all samples due to rod-shaped NPs and reduced electron-hole recombination, which was accessed by the photodegradation of Rhodamine B (RhB).

1. Introduction

Environmental pollution has been triggered by countless dangerous organic pollutants, which are emitted by various chemical enterprises, pharmaceutical firms, chemical dye factories, and so on [1]. Discharge of these pollutants into the hydrosphere, as well as atmosphere, poses a threat to the ecological equilibrium of the Earth as well as human being. The fact that these complex chemicals have been discovered in wastewater as well as drinking water supplies is alarming. Multiple techniques, such as physical, biological, and chemical procedures with a variety of sub-techniques, are utilized to tackle the problem [2]. However, difficulties connected with them include imbalanced removal of all pollutants, ideal pH and temperature management, and pollutant transfer without breakdown [3]. As a result, all of these have ceased to make way for more efficacious, cost-effective, and plentiful methods, and photocatalytic degradation stands out with limitless applications. Photocatalysis as a water treatment technique has received widespread interest due to its efficacy, ease of operation, and ability to produce non-toxic products [4,5].

Photocatalysis is typically based on the semiconductor photocatalyst nanoparticles' ability to absorb light which causes the electron to be excited from a lower to a higher energy band, resulting in the generation of an electron-hole pair [6,7]. But implementation of the photocatalytic technique is hampered by the rapid recombination of photoinduced e^-/h^+ pairs, which may hinder the

* Corresponding author.
E-mail address: mbillah@mme.buet.ac.bd (M.M. Billah).

https://doi.org/10.1016/j.heliyon.2023.e20948
Received 9 June 2023; Received in revised form 10 August 2023; Accepted 11 October 2023
Available online 12 October 2023

redox process in photocatalysis [8,9].

Among semiconductor photocatalysts (ZnO, TiO_2, Fe_2O_3, CdS, ZnS, etc.), ZnO is a potential candidate for photocatalysis due to their cost-effectiveness, non-toxicity, outstanding chemical and physical stability, and superior light absorption efficacy [10–13]. Furthermore, due to the large exciton binding energy (60 MeV) and wide band gap (3.37 eV), ZnO NPs are developing as a promising candidate for various applications, including optoelectronics, photonics, spintronics, photocatalysis, and gas sensing [4,14–17]. However, ZnO nanoparticles also have the weakness of a high recombination rate of e^-/h^+, which can slow down the photodegradation process [18]. Various approaches have been used to increase the photodegradation of ZnO, including non-metal doping [19], inclusion of transition metals [20], and coupling with other semiconductors [21,22]. However, doping with transition metal are severely limited by their thermal instability and increased recombination of charge carriers [23]. The challenges involved in coupling with other semiconductors include complicated preparation methods, lower yield, and higher energy consumption [24]. So, non-metal doping has emerged as a suitable method to counter the limitations of pristine ZnO [25].

Non-metal doping, i.e., nitrogen and fluorine, has the potential to solve the recombination issue between electrons and holes by trapping electrons or holes [26]. Several studies have been published on N-doped ZnO owing to its potential applications of photodegradation of organic dyes using different synthesis procedures [27–31]. Sun et al. synthesized N-doped ZnO NPs by solvothermal route, which showed improved photocatalytic activities than pure ZnO NPs for methyl orange dye degradation under sunlight irradiation [27]. Lavand et al. also observed improved absorption ability of N-doped ZnO NPs prepared by microemulsion method [28]. Rajbongshi et al. employed sol-gel method to produce N-doped ZnO NPs and found that substitutional nitrogen doping in ZnO might boost photocatalytic activities by increasing the absorption properties of ZnO under solar radiation [29].

Chemical co-precipitation approach has various distinct advantages compared to other processing methods, i.e., complete integration of the dopant into the crystal lattice, control over temperature, solution pH, dopant amount, and rate of mixing [32–36]. This method offers the production of high-purity nanomaterials through environment friendly path, eliminating the use of toxic organic solvents, high pressure, and temperature [37–39]. But only a few studies on N-doped ZnO have been reported so far synthesized by the chemical co-precipitation technique. Kumari et al. used the chemical co-precipitation technique to examine the effect of N-doping on the structural and optical properties of ZnO NPs [40]. Other authors studied the defect states in ZnO crystal lattice after N-doping [41]. However, none of the studies have investigated the impact of varying nitrogen dopant concentrations on the photocatalytic activities of ZnO NPs synthesized by the chemical co-precipitation technique. Inspired by these gaps, and considering the potential enhancement of photodegradation in ZnO through N-doping, we opted for simple and cost-effective chemical co-precipitation method using urea as nitrogen source to synthesize a series of N-doped ZnO NPs, and investigated the photocatalysis activities. Urea is selected as the nitrogen source due to its ability to undergo a reaction in solution, resulting in the production of CO_2 and ammonia [6,7]. The CO_2 generated further contributes to the formation of a carbonate ion (CO_3^{2-}), which plays a crucial role in ZnO formation, while the ammonia molecules serve as the essential source of N atoms [8]. Because NH_3 exhibits a significantly lower N–H bonding energy, the decomposition of NH_3H_2O becomes the primary nitrogen source during the formation of N doped ZnO NPs. In this work, both pristine and N-doped NPs were produced and analyzed using a variety of characterization techniques and studied UV-induced photodegradation of RhB as an organic pollutant.

2. Experimental aspects

2.1. Materials

Zinc nitrate hexahydrate ($Zn(NO_3)_2{\cdot}6H_2O$, Merck-India, assay 96 %) and Urea, ($CO(NH_2)_2$, Merck-India, assay 99 %) were used without further purification as a precursor for N-doped ZnO where NaOH was employed as the precipitating agent. For preparing the aqueous solutions, de-ionized (DI) water was used. Rhodamine B (RhB) was used as a standard organic dye for photocatalytic activity measurement.

2.2. Preparation of nanoparticles

First, 0.02 M $Zn(NO_3)_2{\cdot}6H_2O$ aqueous solution was prepared using DI water, and preferred amount of urea was added while magnetically stirred continuously. 0.08 M NaOH solution was added dropwise to this solution while it was continuously stirred until the pH reached 7. The precipitates were settled overnight and separated by centrifuging at 5000 rpm. Later, the precipitates underwent multiple rinses with deionized water followed by a final rinse with ethanol. After drying overnight, precipitates were crushed using a mortar and then annealed at 500 °C in ambient condition for 2 h.

2.3. Materials characterization

For structural characterization, XRD machine (Empyrean, Panalytical-Netherlands) was employed using Cu-$K_{\alpha 1}$ X-ray ($\lambda = 1.5406$ Å). XRD was carried out between Bragg's angles of $2\theta = 20°–80°$. Field emission scanning electron microscope was employed for the morphological analysis (FESEM: JEOL, JSM, 7600F). The X-ray photoelectron spectra (XPS) were obtained using a K-Alpha Thermo Scientific XPS-spectrometer where Al K_α radiation (E = 1486.6 eV) was used. A PerkinElmer Lambda 365 spectrophotometer was used to get the diffuse reflective spectra (DRS) to calculate the band gap of NPs. The photoluminescence (PL) study was carried out with a spectrophotometer (Mini PL 110, Photon systems).

2.4. Photocatalytic degradation Assessment

For photocatalytic investigation, RhB aqueous solution was used under ultraviolet (UV) irradiation. The photocatalytic degradation measurement setup is depicted in Fig. 1. First, a 100 ml quartz beaker was filled with RhB aqueous solution, and the preferred amount of ZnO was added. Before the photoreaction, the RhB solution containing NPs was stirred with a magnetic stirrer within a dark chamber to reach adsorption-desorption equilibrium with ZnO NPs. Following that, the photocatalytic experiment was initiated by exposing the solution to a UV lamp (6W fluorescent, 365 nm wavelength). Degradation efficiency was measured by taking a 6 ml suspension sample at periodic intervals, and then particles were separated by centrifuging. Finally, the absorbance peak (553 nm) of RhB was measured with a UV spectrophotometer, which was used to measure the degrading efficiency of photocatalysts from Eq. (1).

$$\text{Degradation Efficiency}, \% = \left(1 - \frac{C}{C_0}\right) * 100\% = \left(1 - \frac{A}{A_0}\right) \quad (1)$$

where, C_0 and C represent dye concentrations before and after degradation, whereas A_0 and A represent dye absorbance before and after degradation.

3. Results and discussion

3.1. XRD analysis

Fig. 2 depicts the XRD patterns of ZnN_xO_{1-x} (x = 0, 0.005, 0.01, and 0.02) NPs. The diffraction peaks for crystalline planes found at different 2θ values are nearly perfectly matched with JCPDS card 36–1451, confirming the formation of hexagonal wurtzite ZnO crystal structure [42]. The absence of any secondary phase diffraction peak suggests that N were completely integrated into ZnO matrix. The intensity of major diffraction peaks diminished with increasing N dopant concentration, showing a reduction in crystallinity. This is mainly because of the substitution of O^{2-} (1.26 Å) by N^{3-} (1.32 Å), which created lattice disorder in the crystal [43]. Table 1 presents the reduction in crystallinity, from 90.1 % for pure ZnO to 82.1 % for 2 mol.% N-doped ZnO NPs.

The crystallite size of the samples was measured using Williamson-Hall plot and Scherrer formula using Eqs. (2) and (3), respectively, which are listed in Table 1 [44,45].

For W–H plot, the following Eq. (2) was used.

$$\beta \text{Cos}\theta = K\lambda/D + 4\varepsilon \text{Sin}\theta \quad (2)$$

For Scherrer formula, the following Eq. (3) was used

$$D = k\lambda/\beta \cos\theta \quad (3)$$

in both cases,

D = average size of crystallite in nm

λ = 0.15406 nm (Cu X-ray).

K = crystallite shape factor (0.9).

β = FWHM, θ = Bragg's angle, both in radians.

From the W–H plots in Fig. 3(a–d) for pure and N-doped ZnO NPs, crystallite size (D) was calculated from the y-intercept, while strain (ε) was calculated from the slope of βCosθ vs. 4Sinθ. The crystallite size was gradually reduced from 27.7 nm to 20.8 nm after 2 mol.% N-doped ZnO NPs, respectively. Full width at half maximum (FWHM) values increased for all planes with increasing dopant concentration, indicating a decrease in average crystallite size [46–48]. Crystallite size was also computed using the Scherrer formula, which showed a similar trend with increasing dopant concentration. The reduction in crystallite size is due to Zn–N formation on the surface of the doped products, which hinders ZnO crystal growth. This is because Zn–N (1.88 Å) is smaller in size compared to Zn–O

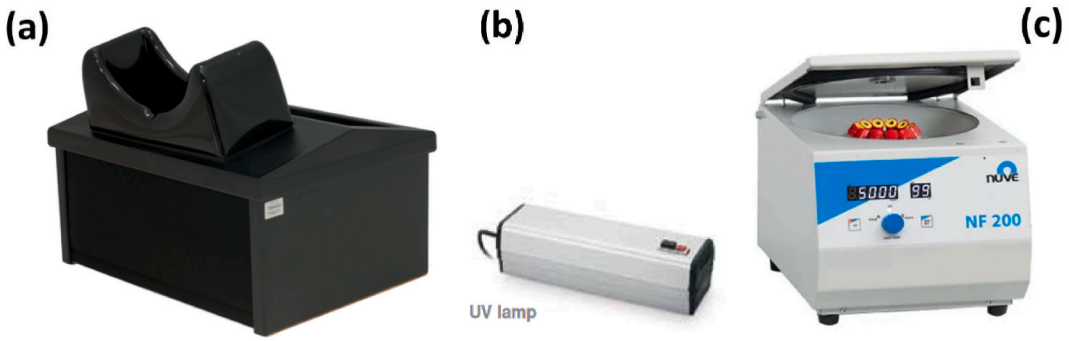

Fig. 1. Photocatalytic measurement setup: (a) Dark box, (b) UV lamp, (c) Centrifuge.

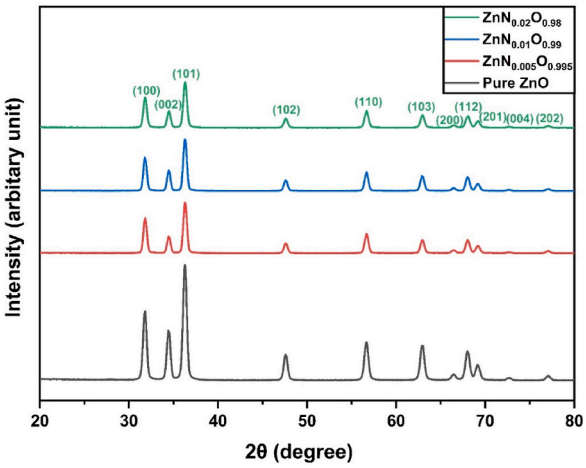

Fig. 2. XRD patterns of ZnN_xO_{1-x} (x = 0, 0.005, 0.01, and 0.02) NPs showing hexagonal wurtzite structure.

Table 1
Crystallinity data and lattice parameters of ZnN_xO_{1-x} (x = 0, 0.005, 0.01, and 0.02) NPs.

Composition	Average crystallite size (nm)		Micro-strain, $*10^{-4}$	Percentage of crystallinity	Lattice parameter (Å)		c/a
	W–H plot	Scherrer equation			a	c	
ZnO	27.7	24.2	8.77	90.1	3.2510	5.2072	1.6017
$ZnN_{0.005}O_{0.995}$	24.1	21.0	8.92	87.4	3.2511	5.2080	1.6019
$ZnN_{0.01}O_{0.99}$	22.7	20.1	9.28	85.2	3.2510	5.2080	1.6020
$ZnN_{0.02}O_{0.98}$	20.8	18.1	5.55	82.1	3.2490	5.2038	1.6017

(1.93 Å), and this size difference plays a key role in decreasing the crystallite size [49,50].

The calculated micro-strain from the W–H plot exhibited an initial increase up to 1 mol.% nitrogen doping, followed by a subsequent decrease. Doping generated lattice disorder, due to size mismatch, leading to stress generation and consequently an increase in the average micro-strain increased [51–53]. However, micro-stain decreased with 2 mol.% doping, possibly due to lattice shrinkage, as supported by the lattice parameter values provided in Table 1.

The Rietveld fitted curves of all samples are shown in Fig. 4(a–d). Lattice parameter values suggest that initial N doping in ZnO led to expansion along the c-axis which is consistent with an earlier report on N-doped ZnO [54]. This was primarily attributed to urea which potentially accelerated the formation of ZnO crystal along the c-axis direction [55]. But higher doping (2 mol.%) might inhibit the c-axis direction crystal growth because of the formation of short-length Zn–N bonds compared to the Zn–O bonds [49,50,56].

3.2. XPS analysis

Fig. 5(a) depicts survey scans of pure and 1 mol.% N-doped ZnO NPs, which show characteristic peaks of various elements present in the samples. The binding energy values of Zn (2p 1/2, 2p 3/2) and O 1s are around 1044.08 eV, 1020.98 eV, and 530.08 eV, respectively, which resembles the ZnO wurtzite structure [57,58]. C 1s peak was detected at about 286 eV binding energy, which could be associated with carbon on the surface caused by contamination from exposure to the outside environment. Also, several auger emissions were found in the XPS scan, which was identified as O KLL, Zn LMM, Zn L3MM, Zn L2MM [59]. A distinct region corresponding to N 1s was detected within the range of approximately 396 eV–402 eV, providing clear evidence of the presence of nitrogen in N-doped ZnO samples. To provide additional support for the investigations, a high-resolution scan was performed to obtain core-level spectra.

High resolution characteristic XPS peaks of N 1s are depicted in Fig. 5(b) where the peak at 398.4 eV is attributed to O–Zn–N, which is regarded as a substitutional impurity [26]. Fig. 5(c) shows high resolution peaks of Zn 2p of pure and $ZnN_{0.01}O_{0.99}$ NPs. N doping shifts both Zn 2p peaks to slightly lower binding energies due to the electronic interaction between N^{3-} ions and ZnO matrix. In both cases, the gap between these two peaks was calculated to be 23.1 eV.

The deconvolution of the O 1s peak of both pure and nitrogen-doped ZnO NPs revealed four separate fitted peaks, which are shown in Fig. 6(a and b). At 530 eV, a peak was observed for ZnO and $ZnN_{0.01}O_{0.99}$ NPs, corresponding to lattice O_2 ions (O_L), while the fitted peak at about 531 eV was associated with O_2 vacancies (V_O). At higher binding energies (around 531.98 eV and 533.28 eV), two fitted peaks were observed for both ZnO and $ZnN_{0.01}O_{0.99}$ NPs, which correspond to chemisorbed hydroxyl groups from water (O_H) and separated weakly bonded surface oxygen (O_a) [59,60]. Here, O_H (calculated from the ratio of peak area and total O 1s area) increased from 11.71 % to 12.07 % after N-doping. This increase in O_H content, attributed to ZnO surface defects, facilitates the capture of holes,

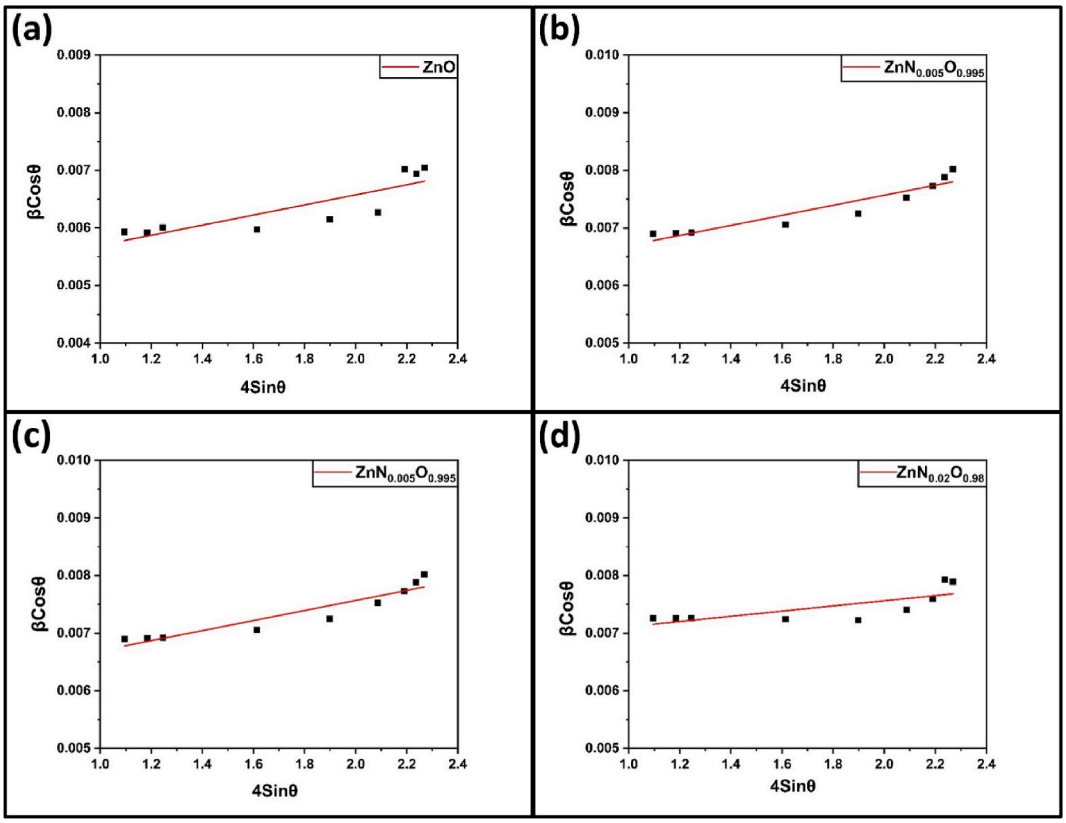

Fig. 3. Williamson-Hall plot of (a) ZnO, (b) $ZnN_{0.005}O_{0.995}$, (c) $ZnN_{0.01}O_{0.99}$, (d) $ZnN_{0.02}O_{0.98}$ NPs for micro-strain and crystallite size calculation.

leading to the formation of hydroxyl radicals (•OH). These hydroxyl radicals play a crucial role in photodegradation, thereby enhancing the overall photocatalytic activities [61,62].

3.3. Morphological analysis

The SEM images of ZnN_xO_{1-x} (x = 0, 0.005, 0.01, and 0.02) NPs are shown in Fig. 7(a–d). Due to urea-induced crystal growth along the longitudinal c-axis, the morphology of ZnO particles after N doping changed from spherical to rod-shaped [55]. The change of shape can be explained by considering the polar surfaces of ZnO NPs. ZnO possesses a hexagonal structure with alternating planes composed of tetrahedrally coordinated O^{2-} and Zn^{2+} ions [63]. Introducing N^{3-} into the ZnO matrix creates planar defects along these planes, potentially increasing the surface energy and promoting rapid anisotropic growth along various directions while preserving the inherent polarity of the nanostructures [64]. The particle-size analysis of all samples are shown in Fig. 7(e–h). For doped ZnO NPs, the average rod diameter gradually decreased with increasing N concentration. Similar results on ZnO nanorods have also been reported by other authors [65,66]. With increasing N concentration, the formation of short-length Zn–N bonds increased more than Zn–O bonds, which might inhibit crystal growth along the c-axis [67]. Therefore, nitrogen doping initially increased ZnO NPs' diameter from 100 nm to 172 nm due to nanorod formation and eventually decreased the diameter up to 141 nm for 2 mol.% N doped ZnO NPs.

3.4. UV–vis spectroscopy

Diffuse reflectance spectra of ZnN_xO_{1-x} (x = 0, 0.005, 0.01, and 0.02) NPs are depicted in Fig. 8. The absorption threshold of pristine and N-doped ZnO was observed to be approximately 370 nm, indicating a significant UV absorption band. Visible light reflectance dropped slightly, accompanied by a subtle redshift for up to 1 mol.% N-doped ZnO NPs, resulting in a narrower band gap [68].

The direct optical bandgap, E_g value for all samples was obtained using the Kubelka-Munk formula [69]. Fig. 9(a–d) depicts that E_g gradually decreased from 3.243 eV to 3.223 eV after 1 mol.% N-doping. This is mainly because of the creation of shallow acceptor states right above the valence band (VB) due to localized anionic defect states by nitrogen substituting lattice oxygen [66,70–74]. The band gap slightly widened for 2 mol.% N doping, likely resulting from the generation of nitrogen defect states that act as electron-hole recombination centers, lowering absorbability [75–78].

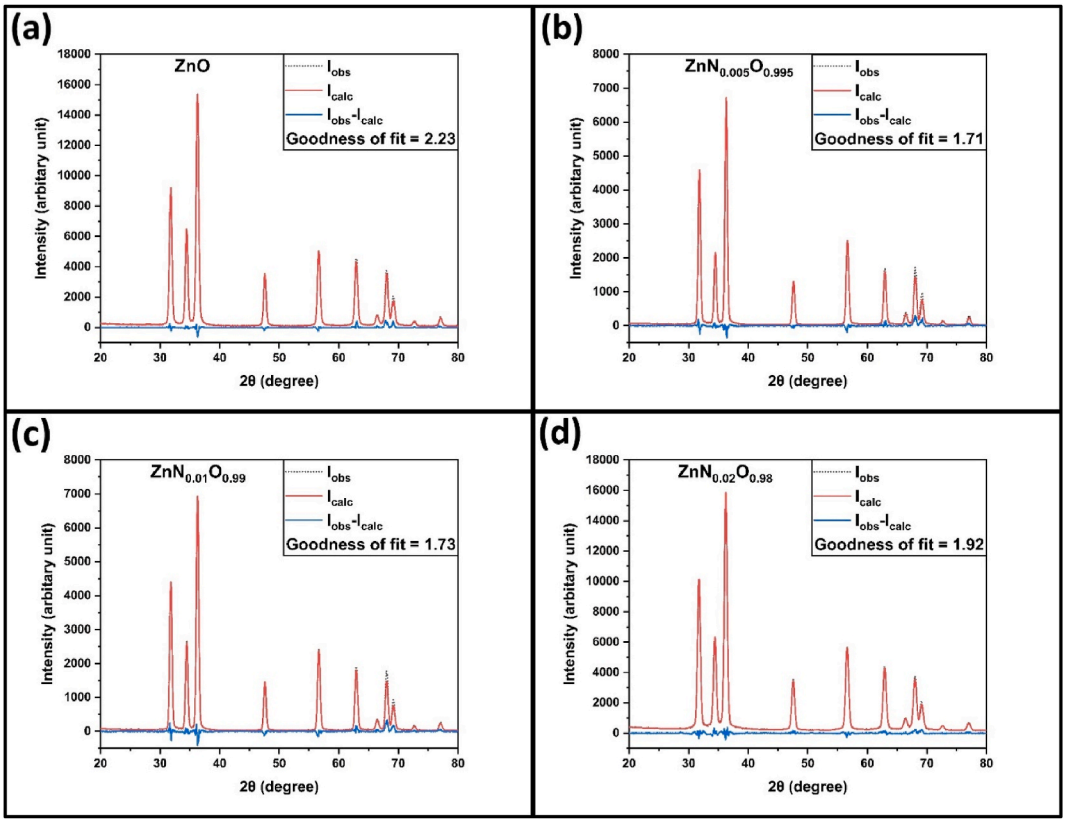

Fig. 4. Rietveld fitted curves of (a) ZnO, (b) $ZnN_{0.005}O_{0.995}$, (c) $ZnN_{0.01}O_{0.99}$, (d) $ZnN_{0.02}O_{0.98}$ NPs.

3.5. PL spectroscopy

The photoluminescence (PL) spectra were analyzed to determine the luminescence properties and probable defect states using an excitation wavelength (λ_{exc}) of 230 nm. PL spectra were normalized with the highest peak at 460 nm, which is the second harmonic PL peak of excitation wavelength (230 nm) (Fig. 10(a)). From the PL spectra of ZnO NPs, typically, two emission bands were detected. The first one is near-band-edge emission (NBE) which appears mainly in the UV region (between 375 and 425 nm) and is attributed to mechanisms that include excitonic collisions [79]. The second in the visible spectrum is deep-level emission (DLE), which is primarily caused by the recombination of photogenerated electron holes resulting from point and surface defects (i.e., V_O, Zn_i) [80,81]. The band gap value from NBE PL spectra was calculated around 3.1–3.2 eV, which is highly correlated to the value calculated from DRS spectra. A slight shift of the NBE peak towards a higher wavelength with nitrogen doping indicates band gap narrowing, which also matches well with UV–vis analysis.

The broad emission band in the visible spectrum consists of multiple peaks. The strongest peak at 460 nm is mainly due to the second harmonic PL peak of excitation wavelength (230 nm) [82]. The violet-blue emission at around 410–490 nm has distinct peaks at 428 nm, 440 nm, and 488 nm, which is typically caused by zinc interstitial (Zn_i) defects [83]. The green emission at around 510–570 nm might be caused by oxygen vacancies (V_o) [84]. The existence of multiple green emissions at 515 nm and 535 nm might be caused by the various narrow energy levels that are nearby to one another inside the band gap [85,86]. The yellow-orange emission at around 570 nm and 600 nm is due to oxygen interstitial (O_i^{2-}) defects [87].

Intense PL peaks indicate intense visible luminescence caused by radiative recombination between distinct metastable defect states. From Fig. 10(a and b), the intensity of all the DLE peaks reduced up to 1 mol.% N doping, indicating that the electron-hole recombination rate is continually reduced [88,89]. The introduction of N dopants can create non-radiative recombination centers that trap excitons, hindering their radiative recombination and resulting in a decrease in photoluminescence (PL) intensity [29]. For 2 mol.% N doping, the intensity of the peaks slightly increased, which suggests a slightly increased recombination rate. This could be because defect states are being eliminated, or defect states are serving as a recombination center for increased doping [90,91].

Fig. 10(c) illustrates the CIE (International Commission on Illumination)1931 diagram of pure and N-doped ZnO NPs. The CIE color chromaticity coordinates were determined through CIE calculation software. For pure ZnO NPs, the coordinates were found to be (x, y) = (0.18, 0.16) [92]. However, a noticeable shift in chromaticity coordinates was observed in N doped ZnO NPs. From the Figure, it becomes evident that the CIE chromaticity coordinates for pure ZnO NPs fall within the blue region, whereas for N-doped ZnO NPs, the color shifts towards an even more pronounced blue emission region [65]. Therefore, N-doped ZnO samples show strong UV emission,

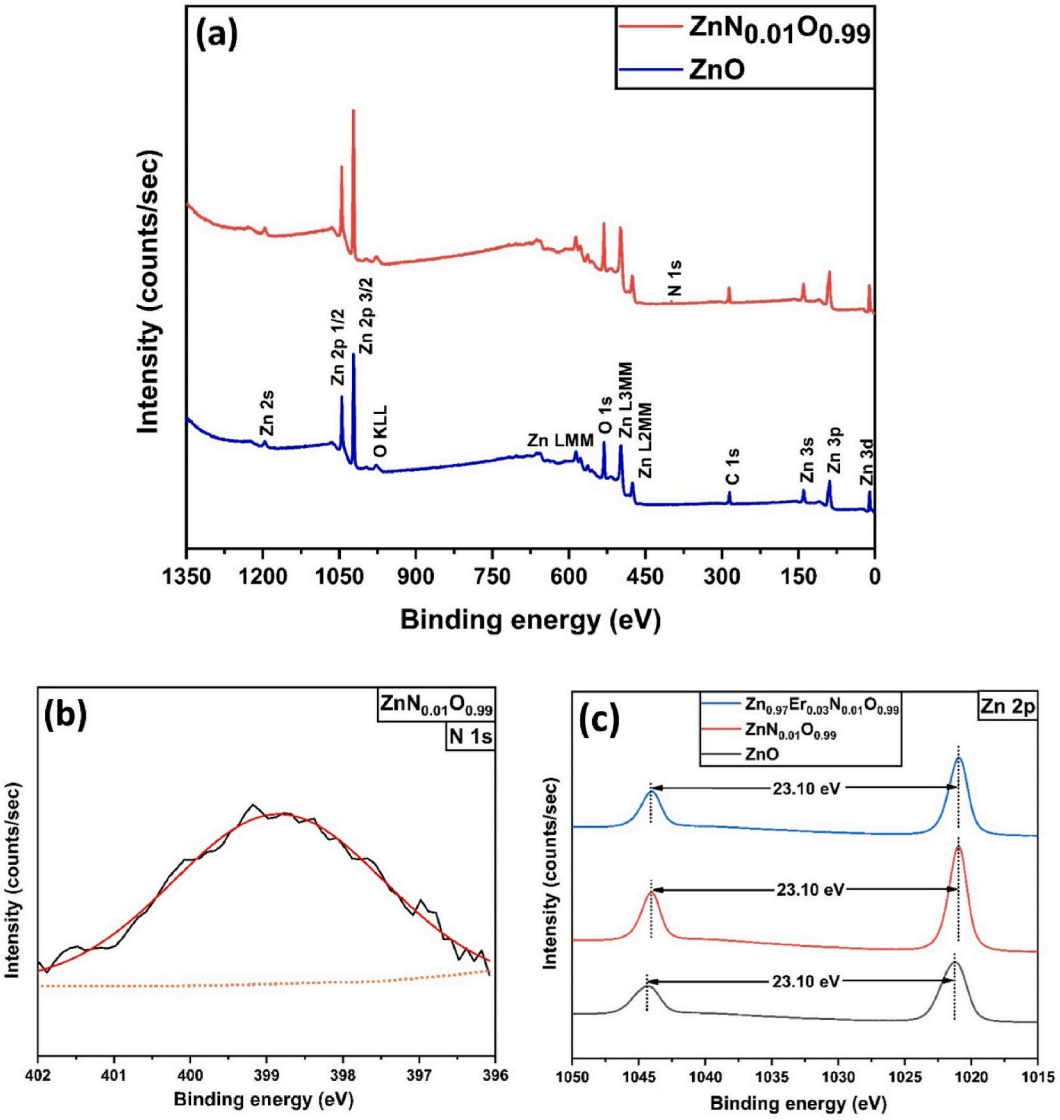

Fig. 5. (A) Survey scan of ZnO and $ZnN_{0.01}O_{0.99}$ NPs; XPS high resolution spectra of (b) N 1s, and (c) Zn 2p states.

making them suitable for use in UV-light emission devices.

3.6. Photocatalytic activity

Fig. 11(a–d) depicts the absorption spectra of Rhodamine B for ZnN_xO_{1-x} (x = 0, 0.005, 0.01, and 0.02) NPs at regular time intervals. Under UV light, the RhB absorption peak at 553 nm was consistently decreased for all samples. However, in the case of N-doped ZnO NPs, the absorbance intensity of RhB decreased more rapidly compared to pure ZnO NPs. For better comparison, C/C_o, and dye degradation were calculated using Eq. (1) and plotted versus reaction time for all the samples, as shown in Fig. 12[(a), (b)].

The plots indicate that nitrogen-doped ZnO NPs are far better photocatalysts than pristine ZnO NPs for degrading RhB dyes. The formation of ZnO nanorod due to N-doping and other factors, such as crystal growth directions, chemisorbed hydroxyl (OH) groups, and defect states of N near valence band, greatly influenced photocatalytic activities of N-doped ZnO NPs. Compared to pristine ZnO spherical particles, which mainly were formed with an exposed (001) plane, the crystal growth orientation of N-doped ZnO nanorods was along the c-axis, that is, [001] direction. It was reported in several studies that having reasonable charge separation between two polar {001} facets in ZnO nanorod can significantly minimize the possibilities of electron-hole recombination. So, these polar {001} surfaces are considered highly reactive surfaces for increased photocatalytic activity [93,94]. Another factor is that more chemisorbed hydroxyl (OH) groups might be present on the ZnO nanorod's surface than ZnO nanosphere, which is confirmed by the XPS study. These OH groups may easily capture holes, forming hydroxyl radicals (•OH) which might increase photocatalytic activities. The

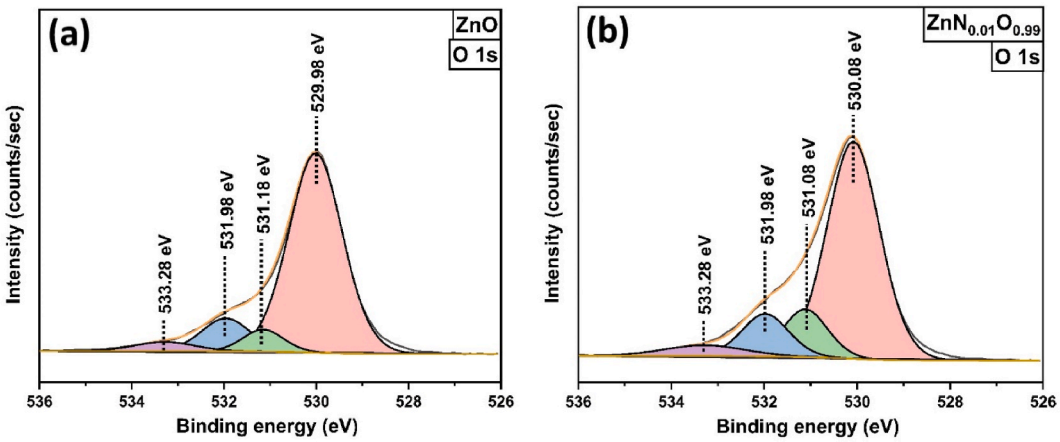

Fig. 6. Deconvoluted XPS scan of O 1s for (a) ZnO, (b) $ZnN_{0.01}O_{0.99}$ NPs.

formation of anionic defect states of N just above VB also plays a vital role for the increased photodegradation of N-doped ZnO NPs by increasing charge separation efficiency, which is evident from PL spectra as well as slightly decreased band gap value after N doping.

From Fig. 12, after 6 h of exposure to UV-light, pure ZnO showed 59 % degradation, whereas for ZnN_xO_{1-x} (x = 0.005, 0.01, and 0.02) NPs, degradation was 81 %, 88 %, and 78 %, respectively. Similar results were also found for the photocatalytic efficiency of N-doped ZnO photocatalysts in the dye degradation as demonstrated in Table 2. 1 mol.% nitrogen-doped ZnO NPs showed better photodegradation because of the formation of long nanorods along the c-axis or [001] direction (evident from lattice parameter c/a ratio) with the primary crystal faces with exposed {100} polar surfaces, which are likely to prevent electron-hole recombination more effectively than pure ZnO [55]. However, 2 mol.% nitrogen-doping decreased photocatalytic activity since higher doping may increase recombination rate, which is confirmed by the PL spectrum of 2 mol.% nitrogen-doped ZnO NPs. This might result from eliminating defect states or acting as a recombination center for higher doping.

3.7. Degradation kinetics

Langmuir-Hinshelwood (L-H) kinetic equation [Eqs. (4)–(6)] was used to simulate how various organic dyes degrade in the presence of semiconductor photocatalysts under illumination. The model states that the photodegradation rate, R, depends upon the percentage of the reactant-covered surface, θ:

$$R = -dC/dt = kr\theta \tag{4}$$

where, C is the reactant concentration, and K_r is the reaction rate constant. The value of θ depends on absorption co-efficient which implies,

$$R = -dC/dt = kr\theta = k_rKC/(1+KC) \tag{5}$$

The equation can be integrated and reduced to a first-order equation for low initial concentration, C_0.

$$\ln(C0/C) = Kt \tag{6}$$

where, K is denoted as the reaction rate constant (first-order).

Fig. 13 depicts a plot of ln (C_0/C) vs. irradiation time for UV-induced RhB photodegradation where all the samples are shown to follow a linear pattern indicating a pseudo-first-order reaction rate. Better photocatalytic effectiveness is correlated with a greater value K, which can be calculated from the slope of each straight line. The K value for pure ZnO NPs was around 0.00258 min^{-1}, while the highest K value was around 0.00563 min^{-1} for $ZnN_{0.01}O_{0.99}$ NPs which indicates around 2.2 times better photocatalytic activities than pristine ZnO NPs.

3.8. Reusability and recyclability test

The reusability and recyclability of 1 mol.% N-doped ZnO photocatalyst were assessed under the same condition. Fig. 14 demonstrates that there is a negligible drop in the photodegradation efficiency for RhB, from 88 % to 81 %, even after undergoing three successive runs. This result indicates that the photocatalyst exhibits promising reusability. Moreover, the photocatalyst can be easily retrieved from the mixtures through a simple centrifugal separation process. These favorable attributes of excellent reusability and recyclability make the photocatalyst well-suited for the purpose of wastewater treatment.

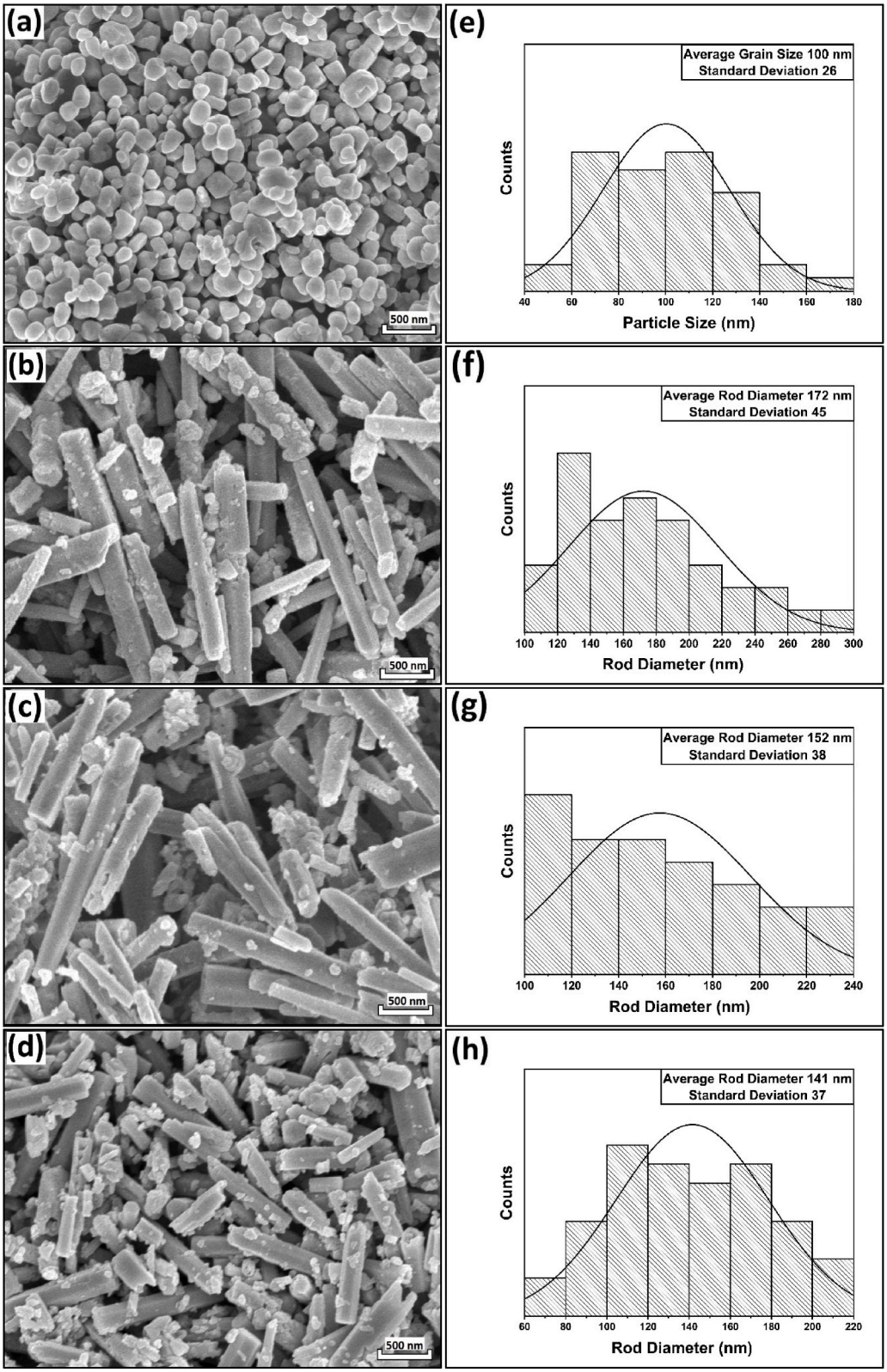

Fig. 7. SEM images (30,000X) of (a) ZnO, (b) $ZnN_{0.005}O_{0.995}$, (c) $ZnN_{0.01}O_{0.99}$, (d) $ZnN_{0.02}O_{0.98}$ NPs; Particle size distribution of (e) ZnO, (f) $ZnN_{0.005}O_{0.995}$, (g) $ZnN_{0.01}O_{0.99}$, (h) $ZnN_{0.02}O_{0.98}$ NPs.

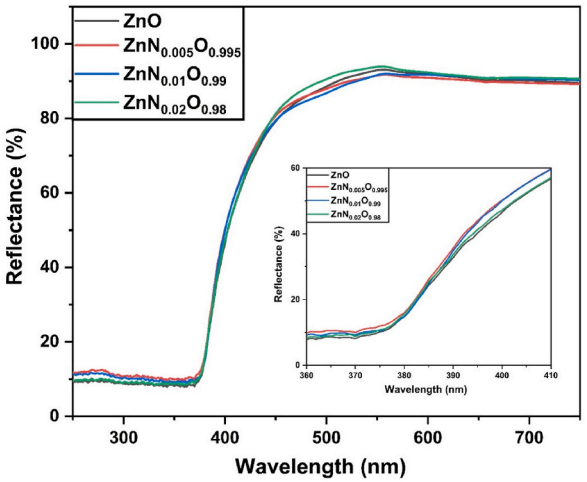

Fig. 8. UV–vis DRS spectra of ZnO, $ZnN_{0.005}O_{0.995}$, $ZnN_{0.01}O_{0.99}$, $ZnN_{0.02}O_{0.98}$ NPs.

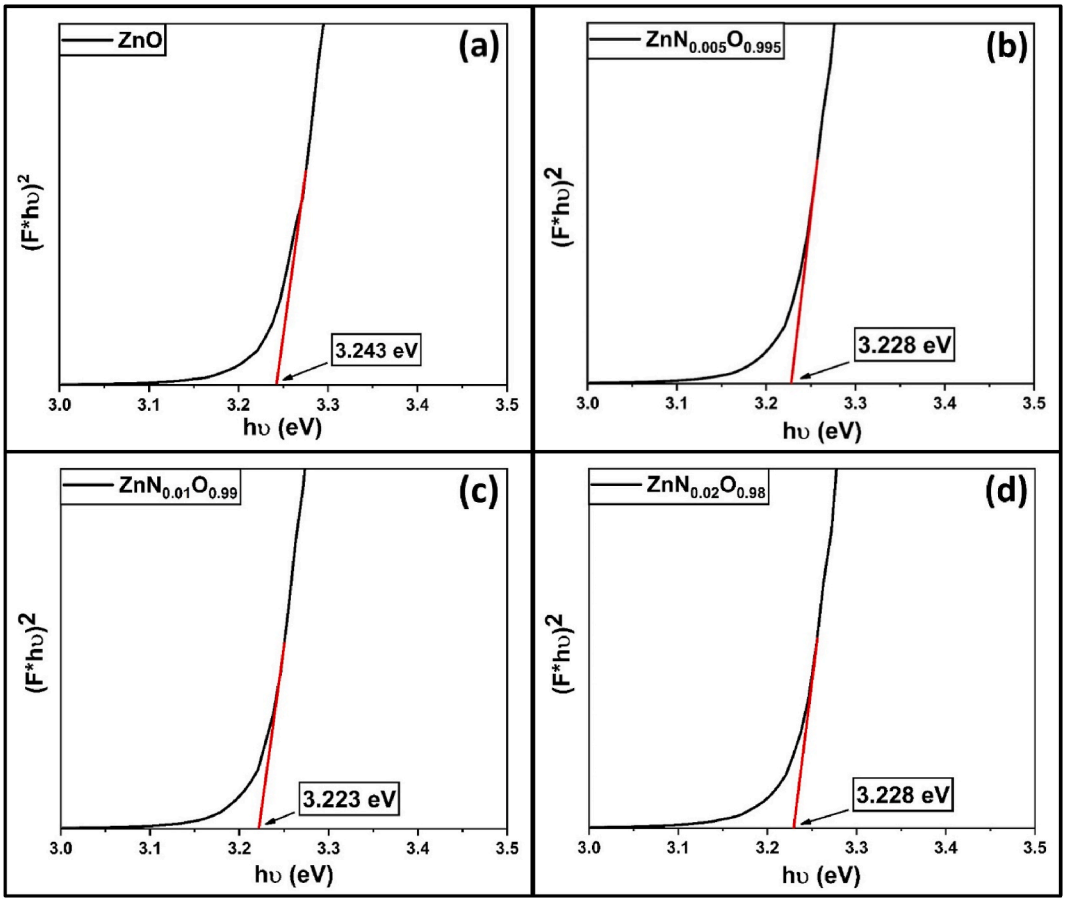

Fig. 9. Direct band gap of (a) ZnO, (b) $ZnN_{0.005}O_{0.995}$, (c) $ZnN_{0.01}O_{0.99}$, (d) $ZnN_{0.02}O_{0.98}$ NPs.

3.9. N-doped ZnO NPs photocatalytic mechanism

A possible mechanism for the increased photocatalytic activities of N-doped ZnO NPs is shown in Fig. 15 by combining the experimental results with the related literature [99,100]. Under UV irradiation ($h\nu \geq E_g$), e^- is promoted to the conduction band from the valence band, forming electron-hole (e^-/h^+) pairs [Eq. (7)]. Substitutional nitrogen doping in ZnO would create new defect states

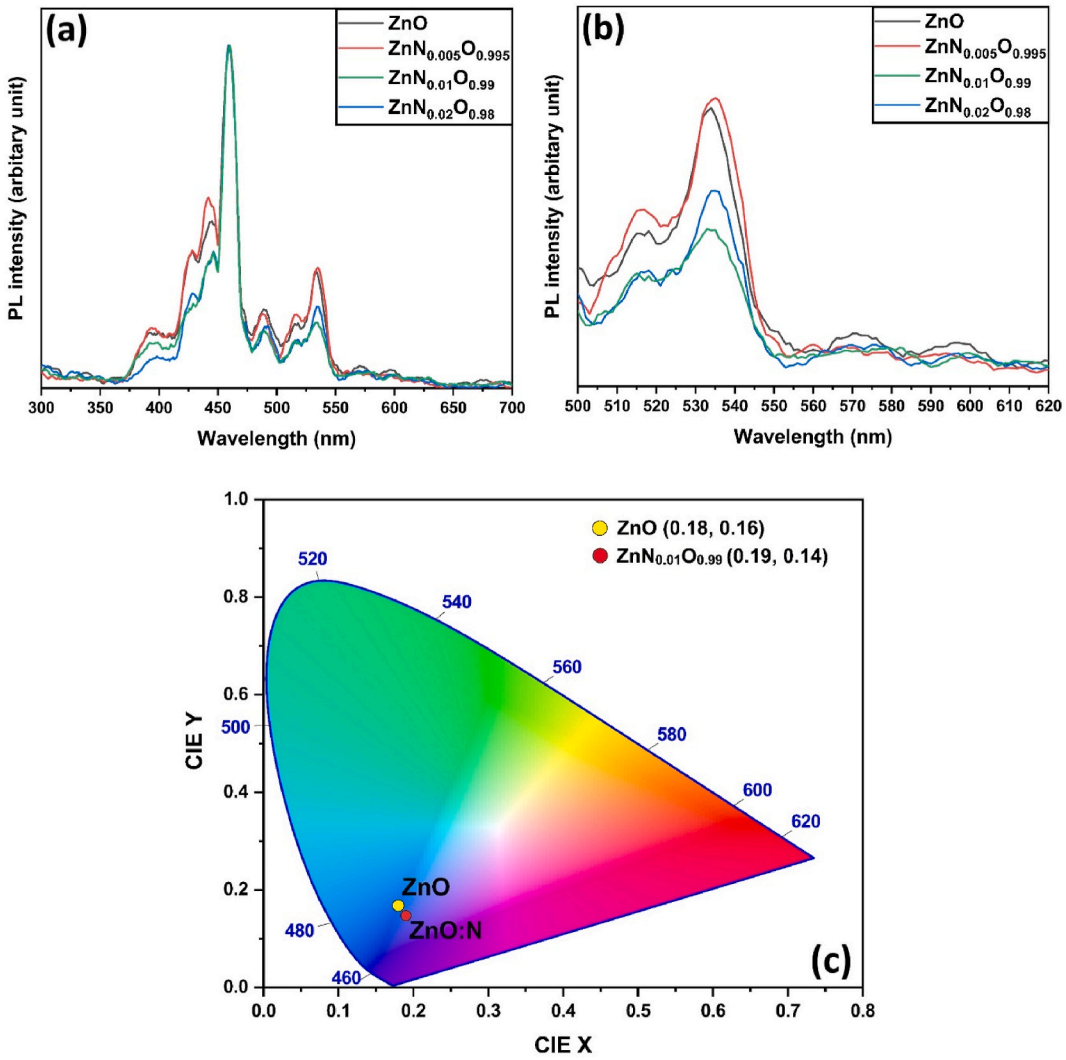

Fig. 10. Photoluminescence spectra from (a) 300–700 nm, (b) 500–620 nm of ZnO, $ZnN_{0.005}O_{0.995}$, $ZnN_{0.01}O_{0.99}$, $ZnN_{0.02}O_{0.98}$ NPs; (c) CIE chromaticity coordinates for ZnO, $ZnN_{0.01}O_{0.99}$ NPs.

just above the valence band, responsible for enhanced photodegradation. These intra-bandgap defect states associated with substitutional N-doping in O sites can exist in either neutral states (N_O^0), or negative charge (−1) states (N_O^-) [101]. The presence of N_O^0 and N_O^- states enhance charge (e^-/h^+) separation efficiency in two steps (electron migration from VB to N defect states, and then to CB) where these defect states work as an intermediate step or "stepping-stone" [Eqs. (8) and (9)] [101,102].

The e^-/h^+ pairs formed after irradiation can quickly move to the ZnO surface and participate in redox processes. Here, e^- combines with O_2 to form superoxide anions radical ($O_2\bullet^-$), which readily reacts with H^+ to produce per hydroxyl free radical ($HO_2\bullet$) and is later converted to hydrogen peroxide (H_2O_2) [Eqs. (10)–(12)]. The hydroxyl radicals are formed when hydrogen peroxide is decomposed by taking e^- from CB or under irradiation [Eqs. (13) and (14)]. On the other hand, h^+ may react with hydroxide ions or direct water to generate hydroxyl (OH•) radicals [Eqs. (15) and (16)]. The generated OH• from redox processes are strong oxidizing agents that target pollutants adsorbed on ZnO, rapidly forming intermediate compounds before being converted to green chemicals like CO_2, and H_2O [Eq. (17)] [103]. The degrading mechanism of N-doped ZnO NPs may be summed up as follows.

$$ZnO + h\nu\ (\text{UV irradiation}) \rightarrow ZnO\ (e^-_{(CB)}) + ZnO\ (h^+_{(VB)}) \quad (7)$$

$$N_O^0 + e^- = N_O^- \text{ (electron migration from VB)} \quad (8)$$

$$N_O^- - e^- = N_O^0 \text{ (electron migration to CB)} \quad (9)$$

$$e^-_{(CB)} + O_2 \rightarrow O_2\bullet^- \quad (10)$$

$$H^+ + O_2\bullet^- \rightarrow HO_2\bullet \quad (11)$$

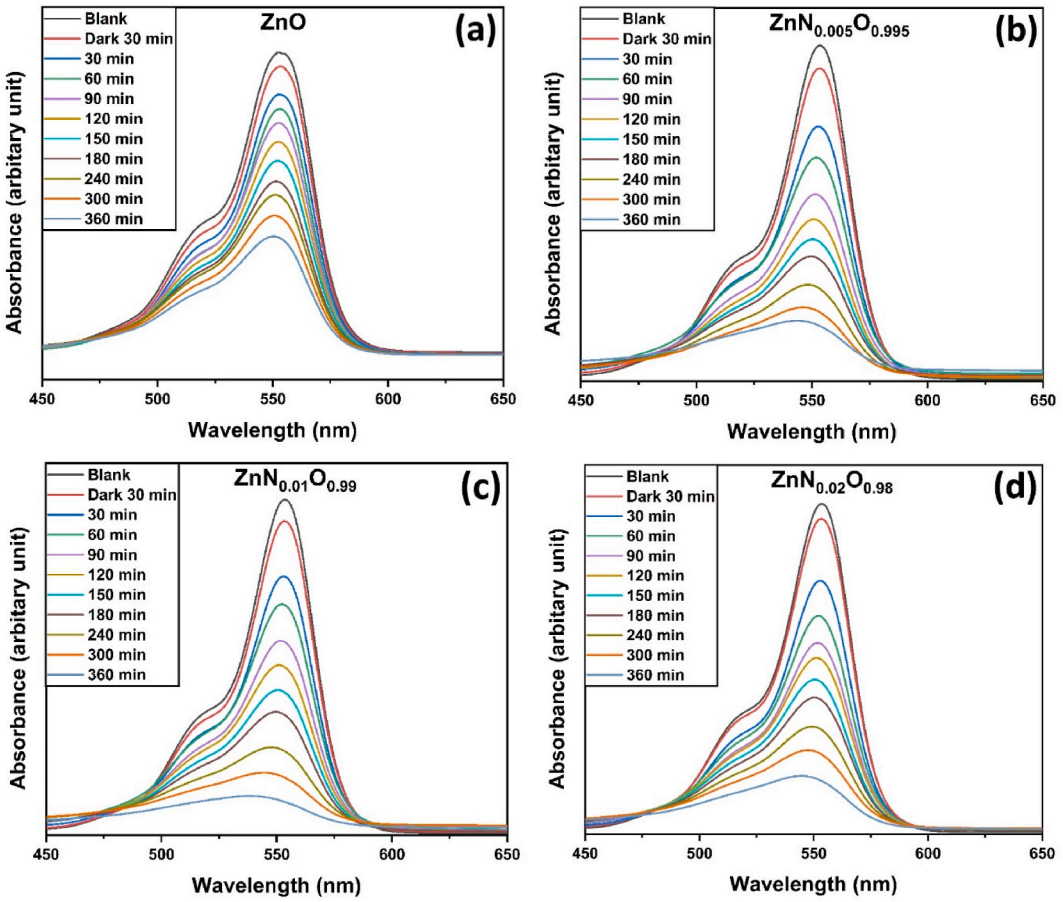

Fig. 11. Time dependent UV–vis absorption spectra of RhB showing photodegradation by (a) ZnO, (b) $ZnN_{0.005}O_{0.995}$, (c) $ZnN_{0.01}O_{0.99}$, (d) $ZnN_{0.02}O_{0.98}$ NPs.

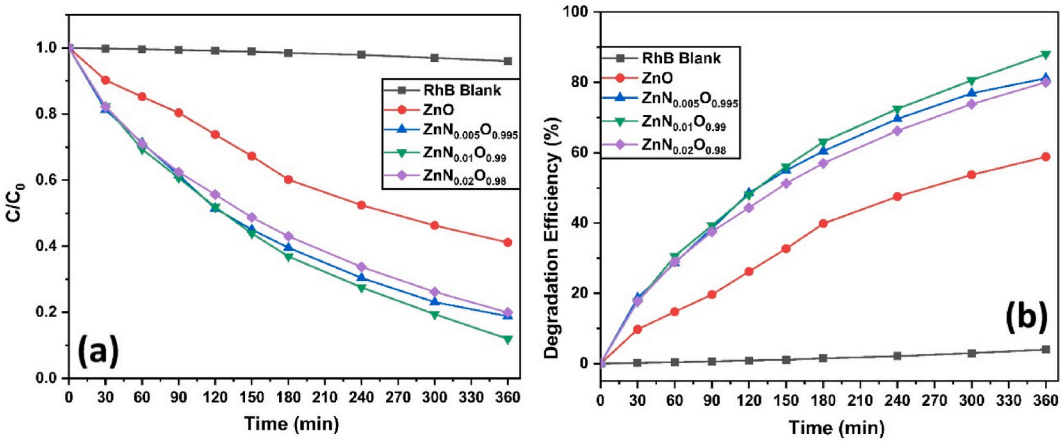

Fig. 12. (A) Remaining concentration of RhB (C/C_o); (b) Degradation efficiency of RhB solution by ZnO, $ZnN_{0.005}O_{0.995}$, $ZnN_{0.01}O_{0.99}$, $ZnN_{0.02}O_{0.98}$ NPs.

$$2HO_2\bullet \rightarrow O_2 + H_2O_2 \quad (12)$$

$$e^-_{(CB)} + H_2O_2 \rightarrow OH\bullet + OH^- \quad (13)$$

Table 2
Comparison of photocatalytic activities of N doped ZnO NPs.

Photocatalyst	Pollutant	Preparation method	Irradiation	Degradation efficiency (%)	Ref.
N doped ZnO NPs	RhB	Citrate precursor method	UV for 120 min	60	[95]
	Thymol blue (TB)	Solid state reaction	UV for 180 min	59.5	[96]
	RhB	Mechanochemical method	UV for 180 min	86 %	[97]
	$K_2Cr_2O_7$	Heat treatment method	UV for 180 min	39 %	[98]
	RhB	Co-precipitation method	UV for 180 min (360 min)	64 % (88 %)	This work

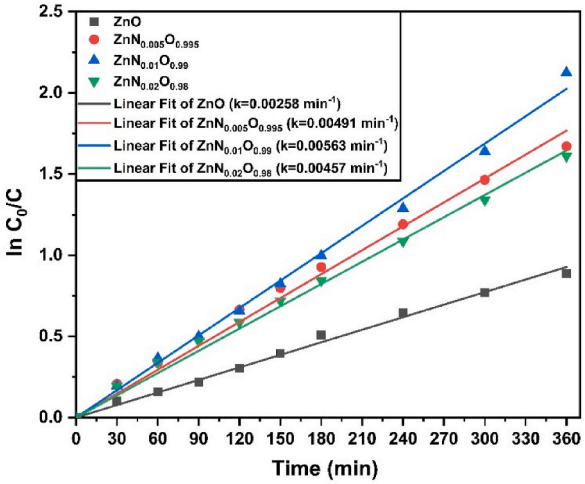

Fig. 13. Kinetics of photodegradation of RhB in the presence of ZnO, $ZnN_{0.005}O_{0.995}$, $ZnN_{0.01}O_{0.99}$, $ZnN_{0.02}O_{0.98}$ NPs.

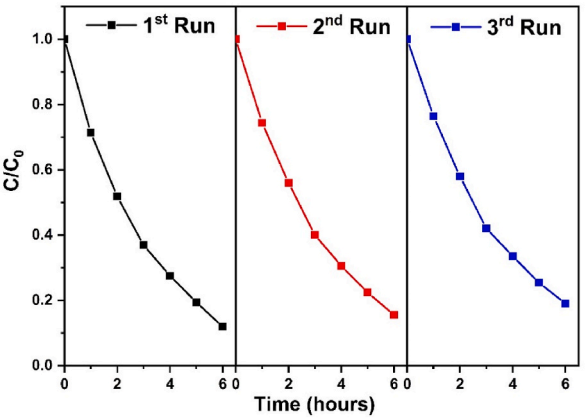

Fig. 14. Reusability and Recyclability test for three successive runs using 1 mol.% N-doped ZnO NPs.

$$H_2O_2 + h\nu \rightarrow 2OH\bullet \quad (14)$$

$$h^+_{(VB)} + OH^- \rightarrow OH\bullet \quad (15)$$

$$h^+_{(VB)} + H_2O \rightarrow H^+ + OH\bullet \quad (16)$$

$$\text{Organic contaminants} + OH\bullet \rightarrow \text{Intermediates} \rightarrow CO_2 + H_2O \quad (17)$$

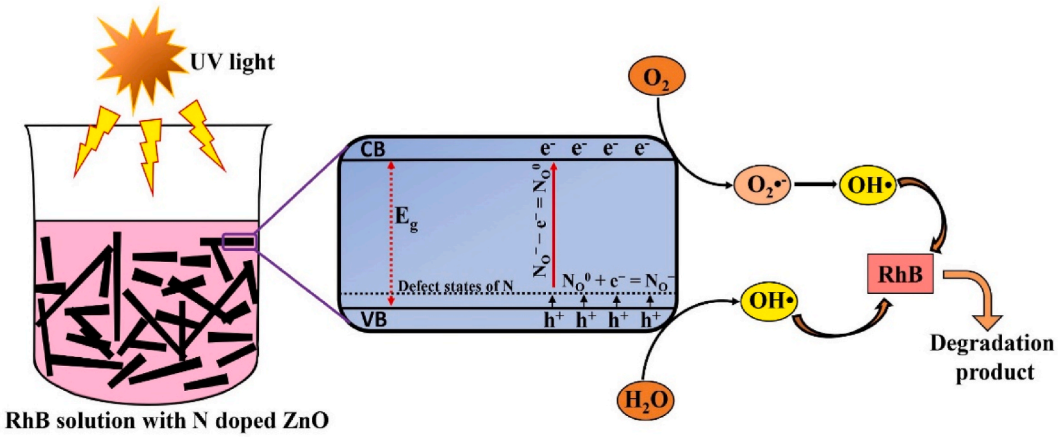

Fig. 15. Schematic representation of possible photodegradation mechanism of RhB dye with N-doped ZnO NPs.

4. Conclusion

In this study, chemical co-precipitation method has been successfully used to synthesize high purity N doped ZnO NPs as potential photocatalysts. XRD and XPS analysis confirmed successful nitrogen doping in ZnO NPs without any secondary phase. SEM images depicted that nitrogen doping changed the shape of ZnO nanoparticles from spherical to nanorods. The average diameter of ZnO nanorod gradually decreased with increasing N concentration. Nitrogen doping boosted photocatalytic activity relative to undoped ZnO NPs up to a certain concentration. 1 mol.% N-doped ZnO NPs showed 2.2 times better photocatalytic activities than pristine ZnO NPs after 6 h under UV irradiation. From SEM images and PL spectra, it was concluded that increased photocatalytic activities are mostly due to nanorod formation, and decreased recombination of e^-/h^+ pairs. Higher doping (2 mol.%) was found to decrease photocatalytic activities because of increased e^-/h^+ recombination. These findings indicate a promising and environmentally favorable synthesis method for the rapid and simple production of photocatalysts, allowing for efficient pollutant elimination.

Declaration of competing interest

The authors declare that they have no known competing financial interests or personal relationships that could have appeared to influence the work reported in this paper.

Acknowledgements

Authors are thankful to the Department of Materials and Metallurgical Engineering, Department of Nanomaterials and Ceramic Engineering, BUET, and Bangladesh Atomic Energy Commission for their support and characterization facilities. Authors are also grateful to the Committee of Advanced Studies and Research (CASR), BUET, for the funding support.

References

[1] M. Osman, Waste water treatment in chemical industries: the concept and current technologies, Journal of Waste Water Treatment & Analysis 5 (2014) 1–12, https://doi.org/10.4172/2157-7587.1000164.
[2] S. Mondal, A. Sharif, Antimicrobial Biocomposites, Elsevier Ltd., 2021, https://doi.org/10.1016/B978-0-12-821553-1.00006-5.
[3] N. Siva, D. Sakthi, S. Ragupathy, V. Arun, N. Kannadasan, Synthesis, structural, optical and photocatalytic behavior of Sn doped ZnO nanoparticles, Mater Sci Eng B Solid State Mater Adv Technol 253 (2020), 114497, https://doi.org/10.1016/j.mseb.2020.114497.
[4] R. Saravanan, H. Shankar, T. Prakash, V. Narayanan, A. Stephen, ZnO/CdO composite nanorods for photocatalytic degradation of methylene blue under visible light, Mater. Chem. Phys. 125 (2011) 277–280, https://doi.org/10.1016/j.matchemphys.2010.09.030.
[5] Z. Abdi, A. Malek Khachatourian, A. Nemati, Visible-light-driven photocatalytic activity of NiFe2O4@Ti-doped ZnO magnetically separable nanoparticles anchored on N-doped rGO nanosheets, Diam. Relat. Mater. 135 (2023), 109839, https://doi.org/10.1016/J.DIAMOND.2023.109839.
[6] N. Kaneva, I. Stambolova, V. Blaskov, Y. Dimitriev, A. Bojinova, C. Dushkin, A comparative study on the photocatalytic efficiency of ZnO thin films prepared by spray pyrolysis and sol–gel method, Surf. Coat. Technol. 207 (2012) 5–10, https://doi.org/10.1016/J.SURFCOAT.2011.10.020.
[7] G. Li, Z. Yi, H. Wang, C. Jia, W. Zhang, Factors impacted on anisotropic photocatalytic oxidization activity of ZnO: surface band bending, surface free energy and surface conductance, Appl. Catal., B 158–159 (2014) 280–285, https://doi.org/10.1016/J.APCATB.2014.04.034.
[8] T. Lv, L. Pan, X. Liu, Z. Sun, Enhanced photocatalytic degradation of methylene blue by ZnO-reduced graphene oxide-carbon nanotube composites synthesized via microwave-assisted reaction, Catal. Sci. Technol. 2 (2012) 2297–2301, https://doi.org/10.1039/c2cy20023f.
[9] J.H. Sun, S.Y. Dong, J.L. Feng, X.J. Yin, X.C. Zhao, Enhanced sunlight photocatalytic performance of Sn-doped ZnO for Methylene Blue degradation, J. Mol. Catal. Chem. 335 (2011) 145–150, https://doi.org/10.1016/j.molcata.2010.11.026.
[10] K. Choi, T. Kang, S.G. Oh, Preparation of disk shaped ZnO particles using surfactant and their PL properties, Mater. Lett. 75 (2012) 240–243, https://doi.org/10.1016/J.MATLET.2012.02.031.
[11] S. Liang, K. Xiao, Y. Mo, X. Huang, A novel ZnO nanoparticle blended polyvinylidene fluoride membrane for anti-irreversible fouling, J. Membr. Sci. (2012), https://doi.org/10.1016/J.MEMSCI.2011.12.040, 394-395184–192.

[12] D.K. Muthee, B.F. Dejene, Effect of annealing temperature on structural, optical, and photocatalytic properties of titanium dioxide nanoparticles, Heliyon 7 (2021), https://doi.org/10.1016/j.heliyon.2021.e07269, 1-7.

[13] L. Soto-vázquez, M. Cotto, C. Morant, J. Duconge, F. Márquez, Journal of Photochemistry and Photobiology A : chemistry Facile synthesis of ZnO nanoparticles and its photocatalytic activity in the degradation of 2-phenylbenzimidazole-5-sulfonic acid, J. Photochem. Photobiol. Chem. 332 (2017) 331–336, https://doi.org/10.1016/j.jphotochem.2016.09.010.

[14] N.A. Yusoff, L.N. Ho, S.A. Ong, Y.S. Wong, W.F. Khalik, Photocatalytic activity of zinc oxide (ZnO) synthesized through different methods, Desalination Water Treat. 57 (2016) 12496–12507, https://doi.org/10.1080/19443994.2015.1054312.

[15] R.D. Suryavanshi, S.V. Mohite, A.A. Bagade, S.K. Shaikh, J.B. Thorat, K.Y. Rajpure, Nanocrystalline Immobilised ZnO Photocatalyst for Degradation of Benzoic Acid and Methyl Blue Dye, Elsevier Ltd, 2018, https://doi.org/10.1016/j.materresbull.2018.01.042.

[16] T. Iqbal, A. Raza, M. Zafar, S. Afsheen, I. Kebaili, H. Alrobei, Plant-mediated green synthesis of zinc oxide nanoparticles for novel application to enhance the shelf life of tomatoes, Appl. Nanosci. 12 (2022) 179–191, https://doi.org/10.1007/s13204-021-02238-z.

[17] T. Iqbal, A. Masood, N.R. Khalid, M.B. Tahir, A.M. Asiri, H. Alrobei, Green synthesis of novel lanthanum doped copper oxide nanoparticles for photocatalytic application: correlation between experiment and COMSOL simulation, Ceram. Int. 48 (2022) 13420–13430, https://doi.org/10.1016/j.ceramint.2022.01.160.

[18] C.B. Ong, L.Y. Ng, A.W. Mohammad, A review of ZnO nanoparticles as solar photocatalysts: synthesis, mechanisms and applications, Renew. Sustain. Energy Rev. 81 (2018) 536–551, https://doi.org/10.1016/j.rser.2017.08.020.

[19] C. Shifu, Z. Wei, Z. Sujuan, L. Wei, Preparation, characterization and photocatalytic activity of N-containing ZnO powder, Chem. Eng. J. 148 (2009) 263–269, https://doi.org/10.1016/j.cej.2008.08.039.

[20] K.G. Kanade, B.B. Kale, J.O. Baeg, S.M. Lee, C.W. Lee, S.J. Moon, H. Chang, Self-assembled aligned Cu doped ZnO nanoparticles for photocatalytic hydrogen production under visible light irradiation, Mater. Chem. Phys. 102 (2007) 98–104, https://doi.org/10.1016/j.matchemphys.2006.11.012.

[21] R. Saravanan, V.K. Gupta, E. Mosquera, F. Gracia, Preparation and characterization of V2O5/ZnO nanocomposite system for photocatalytic application, J. Mol. Liq. 198 (2014) 409–412, https://doi.org/10.1016/j.molliq.2014.07.030.

[22] A. Sharif, S. Mondal, M.E. Hoque, Polylactic Acid (PLA)-based Nanocomposites: Processing and Properties, Bio-Based Polymers and Nanocomposites: Preparation, Processing, Properties & Performance, 2019, pp. 233–254, https://doi.org/10.1007/978-3-030-05825-8_11.

[23] A.E. Ramírez, M. Montero-Muñoz, L.L. López, J.E. Ramos-Ibarra, J.A.H. Coaquira, B. Heinrichs, C.A. Páez, Significantly enhancement of sunlight photocatalytic performance of ZnO by doping with transition metal oxides, Sci. Rep. 11 (2021) 1–9, https://doi.org/10.1038/s41598-020-78568-9.

[24] R. Guan, J. Li, J. Zhang, Z. Zhao, D. Wang, H. Zhai, D. Sun, Photocatalytic performance and mechanistic Research of ZnO/g-C3N4 on degradation of methyl orange, ACS Omega 4 (2019), 20742, https://doi.org/10.1021/acsomega.9b03129. –20747.

[25] F.M. Sanakousar, C. Vidyasagar, V.M. Jiménez-Pérez, K. Prakash, Recent progress on visible-light-driven metal and non-metal doped ZnO nanostructures for photocatalytic degradation of organic pollutants, Mater. Sci. Semicond. Process. 140 (2022), https://doi.org/10.1016/j.mssp.2021.106390.

[26] H. Qin, W. Li, Y. Xia, T. He, Photocatalytic activity of heterostructures based on ZnO and N-doped ZnO, ACS Appl. Mater. Interfaces 3 (2011) 3152–3156, https://doi.org/10.1021/AM200655H.

[27] S. Sun, X. Chang, X. Li, Z. Li, Synthesis of N-doped ZnO nanoparticles with improved photocatalytical activity, Ceram. Int. 39 (2013) 5197–5203, https://doi.org/10.1016/j.ceramint.2012.12.018.

[28] A.B. Lavand, Y.S. Malghe, Synthesis, characterization and visible light photocatalytic activity of nitrogen-doped zinc oxide nanospheres, Journal of Asian Ceramic Societies 3 (2015) 305–310, https://doi.org/10.1016/j.jascer.2015.06.002.

[29] B.M. Rajbongshi, A. Ramchiary, S. Samdarshi, Influence of N-doping on photocatalytic activity of ZnO nanoparticles under visible light irradiation, Mater. Lett. 134 (2014) 111–114, https://doi.org/10.1016/j.matlet.2014.07.073.

[30] E. Prabakaran, K. Pillay, Synthesis of N-doped ZnO nanoparticles with cabbage morphology as a catalyst for the efficient photocatalytic degradation of methylene blue under UV and visible light, RSC Adv. 9 (2019) 7509–7535, https://doi.org/10.1039/C8RA09962F.

[31] S. Monga, N. Sharma, R.K. Choubey, Y.K. Mishra, R.S. Katiyar, A. Singh, Prospects of non-linear optical behaviour of PZT/ZnO heterostructures, Ceram. Int. 49 (2023) 11737–11752, https://doi.org/10.1016/j.ceramint.2022.11.297.

[32] C. Selvaraju, R. Karthick, R. Veerasubam, The modification of structural, optical and antibacterial activity properties of rare Earth gadolinium-doped ZnO nanoparticles prepared by Co-precipitation method, J. Inorg. Organomet. Polym. Mater. 29 (2019) 776–782, https://doi.org/10.1007/S10904-018-1051-0/FIGURES/6.

[33] N. Prasad, B. Karthikeyan, Cu-doping and annealing effect on the optical properties and enhanced photocatalytic activity of ZnO nanoparticles, Vacuum 146 (2017) 501–508, https://doi.org/10.1016/J.VACUUM.2017.03.028.

[34] S. Mondal, S.A. Ayon, M.M. Billah, Comparative Study of Structural, Optical, and Photocatalytic Properties of ZnO Synthesized by Chemical Coprecipitation and Modified Sol–Gel Methods, Surface and Interface Analysis, 2023, pp. 1–6, https://doi.org/10.1002/sia.7210.

[35] S. Kinra, M.P. Ghosh, S. Mohanty, R.K. Choubey, S. Mukherjee, Manganese ions substituted ZnO nanoparticles: synthesis, microstructural and optical properties, Phys. B Condens. Matter 627 (2022), 413523, https://doi.org/10.1016/J.PHYSB.2021.413523.

[36] L.K. Sharma, D. Mandal, R.K. Choubey, S. Mukherjee, On the correlation of the effect of defects on the microstructural, optical and magnetic properties of doped ZnO, Physica E Low Dimens Syst Nanostruct 144 (2022), 115370, https://doi.org/10.1016/J.PHYSE.2022.115370.

[37] C. Pereira, A.M. Pereira, C. Fernandes, M. Rocha, R. Mendes, M.P. Fernández-García, A. Guedes, P.B. Tavares, J.M. Grenéche, J.P. Araújo, C. Freire, Superparamagnetic MFe 2O 4 (M = Fe, Co, Mn) nanoparticles: tuning the particle size and magnetic properties through a novel one-step coprecipitation route, Chem. Mater. 24 (2012) 1496–1504, https://doi.org/10.1021/cm300301c.

[38] S. Kinra, M.P. Ghosh, S. Mohanty, R.K. Choubey, S. Mukherjee, Correlating the microstructural and optical properties of vanadium ion-doped ZnO nanocrystals, Bull. Mater. Sci. 45 (2022), https://doi.org/10.1007/s12034-021-02650-9.

[39] S. Kumar, A. Jain, S. Panwar, I. Sharma, S. Gupta, M. Dopita, R.K. Choubey, Antibacterial studies of ZnO and silica capped manganese doped zinc sulphide nanostructures, Appl. Phys. Mater. Sci. Process 129 (2023), https://doi.org/10.1007/s00339-023-06463-x.

[40] R. Kumari, A. Sahai, N. Goswami, Effect of nitrogen doping on structural and optical properties of ZnO nanoparticles, Prog. Nat. Sci.: Mater. Int. 25 (2015) 300–309, https://doi.org/10.1016/j.pnsc.2015.08.003.

[41] E. Cerrato, A. Privitera, M. Chiesa, E. Salvadori, M.C. Paganini, Nitrogen-doped zinc oxide for photo-driven molecular hydrogen production, Int. J. Mol. Sci. 23 (2022), https://doi.org/10.3390/ijms23095222.

[42] W.Q. Peng, S.C. Qu, G.W. Cong, Z.G. Wang, Structure and visible luminescence of ZnO nanoparticles, Mater. Sci. Semicond. Process. 1 (2006) 156–159, https://doi.org/10.1016/J.MSSP.2006.01.038. –3.

[43] R.D. Shannon, Revised effective ionic radii and systematic studies of interatomic distances in halides and chalcogenides, Acta Crystallogr. A 32 (1976) 751–767, https://doi.org/10.1107/S0567739476001551.

[44] A. Khorsand Zak, W.H. Abd Majid, M.E. Abrishami, R. Yousefi, X-ray analysis of ZnO nanoparticles by Williamson-Hall and size-strain plot methods, Solid State Sci. 13 (2011) 251–256, https://doi.org/10.1016/j.solidstatesciences.2010.11.024.

[45] S. Fatimah, R. Ragadhita, D.F. Al Husaeni, A.B.D. Nandiyanto, How to calculate crystallite size from X-ray diffraction (XRD) using scherrer method, ASEAN Journal of Science and Engineering 2 (2021) 65–76, https://doi.org/10.17509/ajse.v2i1.37647.

[46] S.A. Ansari, A. Nisar, B. Fatma, W. Khan, A.H. Naqvi, Investigation on structural, optical and dielectric properties of Co doped ZnO nanoparticles synthesized by gel-combustion route, Mater Sci Eng B Solid State Mater Adv Technol 177 (2012) 428–435, https://doi.org/10.1016/j.mseb.2012.01.022.

[47] S.A. Ayon, M. Jamal, M.M. Billah, S. Neaz, Augmentation of magnetic properties and antimicrobial activities of band gap modified Ho3+ and Sm3+ doped ZnO nanoparticles: a comparative experimental study, J. Alloys Compd. 897 (2022), 163179, https://doi.org/10.1016/j.jallcom.2021.163179.

[48] S.A. Ayon, S. Hasan, M.M. Billah, S.S. Nishat, A. Kabir, Improved luminescence and photocatalytic properties of Sm3+-doped ZnO nanoparticles via modified sol–gel route: a unified experimental and DFT+U approach, J. Rare Earths 41 (2022) 550–560, https://doi.org/10.1016/j.jre.2022.03.004.

[49] A. Meng, X. Li, X. Wang, Z. Li, CERAMICS Preparation, photocatalytic properties and mechanism of Fe or N-doped Ag/ZnO nanocomposites, Ceram. Int. 40 (2014) 9303–9309, https://doi.org/10.1016/j.ceramint.2014.01.153.

[50] S. Söllradl, M. Greiwe, V.J. Bukas, M.R. Buchner, M. Widenmeyer, T. Kandemir, T. Zweifel, A. Senyshyn, S. Günther, T. Nilges, A. Türler, R. Niewa, Nitrogen-doping in ZnO via combustion synthesis? Chem. Mater. 27 (2015) 4188–4195, https://doi.org/10.1021/CM504200Q/SUPPL_FILE/CM504200Q_SI_003.MPG.

[51] A. Vanaja, G.V. Ramaraju, K. Srinivasa Rao, Structural and optical investigation of Al doped ZnO nanoparticles synthesized by Sol-gel process, Indian J. Sci. Technol. 9 (2016), https://doi.org/10.17485/ijst/2016/v9i12/87013.

[52] K. Jindal, M. Tomar, R.S. Katiyar, V. Gupta, Raman scattering and photoluminescence investigations of N doped ZnO thin films: local vibrational modes and induced ferromagnetism, J. Appl. Phys. 120 (2016), https://doi.org/10.1063/1.4964257.

[53] S.A. Ayon, M. Jamal, A.M. Nahin, M.S. Islam, S.S. Nishat, A. Sharif, Enhanced dielectric stability and coercivity of band gap tuned Ba–Al Co-doped bismuth ferrite: an experimental and DFT+U investigation, Ceram. Int. 48 (2022) 3404–3416, https://doi.org/10.1016/j.ceramint.2021.10.117.

[54] K. Jindal, M. Tomar, V. Gupta, Nitrogen-doped zinc oxide thin films biosensor for determination of uric acid, Analyst 138 (2013) 4353–4362, https://doi.org/10.1039/C3AN36695B.

[55] G. Byzynski, C. Melo, D.P. Volanti, M.M. Ferrer, A.F. Gouveia, C. Ribeiro, J. Andrés, E. Longo, The interplay between morphology and photocatalytic activity in ZnO and N-doped ZnO crystals, Mater. Des. 120 (2017) 363–375, https://doi.org/10.1016/j.matdes.2017.02.020.

[56] X. Zhu, H.-Z. Wu, D.-J. Qiu, Z. Yuan, G. Jin, J. Kong, W. Shen, Photoluminescence and resonant Raman scattering in N-doped ZnO thin films, Optics 283 (2010) 2695–2699, https://doi.org/10.1016/j.optcom.2010.03.006.

[57] M. Chen, X. Wang, Y.H. Yu, Z.L. Pei, X.D. Bai, C. Sun, R.F. Huang, L.S. Wen, X-ray photoelectron spectroscopy and auger electron spectroscopy studies of Al-doped ZnO films, Appl. Surf. Sci. 158 (2000) 134–140, https://doi.org/10.1016/S0169-4332(99)00601-7.

[58] S. Anandan, A. Vinu, K.L.P. Sheeja Lovely, N. Gokulakrishnan, P. Srinivasu, T. Mori, V. Murugesan, V. Sivamurugan, K. Ariga, Photocatalytic activity of La-doped ZnO for the degradation of monocrotophos in aqueous suspension, J. Mol. Catal. Chem. 266 (2007) 149–157, https://doi.org/10.1016/J.MOLCATA.2006.11.008.

[59] A. Sahai, N. Goswami, Probing the dominance of interstitial oxygen defects in ZnO nanoparticles through structural and optical characterizations, Ceram. Int. 40 (2014) 14569–14578, https://doi.org/10.1016/j.ceramint.2014.06.041.

[60] H.B. Fan, S.Y. Yang, P.F. Zhang, H.Y. Wei, X.L. Liu, C.M. Jiao, Q.S. Zhu, Y.H. Chen, Z.G. Wang, Investigation of oxygen vacancy and interstitial oxygen defects in ZnO films by photoluminescence and X-ray photoelectron spectroscopy, Chin. Phys. Lett. 24 (2007) 2108, https://doi.org/10.1088/0256-307X/24/7/089.

[61] Y. Hong, C. Tian, B. Jiang, A. Wu, Q. Zhang, G. Tian, H. Fu, Facile synthesis of sheet-like ZnO assembly composed of small ZnO particles for highly efficient photocatalysis, J Mater Chem A Mater 1 (2013) 5700–5708, https://doi.org/10.1039/C3TA10218A.

[62] W. Lu, S. Gao, J. Wang, One-pot synthesis of Ag/ZnO self-assembled 3D hollow microspheres with enhanced photocatalytic performance, J. Phys. Chem. C 112 (2008) 16792–16800, https://doi.org/10.1021/JP803654K/SUPPL_FILE/JP803654K_SI_001.PDF.

[63] Y.J. Li, C.Y. Wang, M.Y. Lu, K.M. Li, L.J. Chen, Electrodeposited hexagonal ringlike superstructures composed of hexagonal Co-doped ZnO nanorods with optical tuning and high-temperature ferromagnetic properties, Cryst. Growth Des. 8 (2008) 2598–2602, https://doi.org/10.1021/cg7007864.

[64] R. Mahdavi, S.S.A. Talesh, Sol-gel synthesis, structural and enhanced photocatalytic performance of Al doped ZnO nanoparticles, Adv. Powder Technol. 28 (2017) 1418–1425, https://doi.org/10.1016/j.apt.2017.03.014.

[65] S.K. Satpathy, U.K. Panigrahi, S.K. Panda, R. Biswal, W. Luyten, P. Mallick, Structural, optical, antimicrobial and ferromagnetic properties of Zn1−xLaxO nanorods synthesized by chemical route, J. Alloys Compd. 865 (2021), 158937, https://doi.org/10.1016/j.jallcom.2021.158937.

[66] U.K. Panigrahi, M. Barik, S. Hussain, P.K. Satapathy, P. Mallick, Sulphur doping induced band gap narrowing and enhancement of green emission in ZnO nanorods, J. Mater. Sci. Mater. Electron. 33 (2022) 22851–22861, https://doi.org/10.1007/s10854-022-09053-4.

[67] W. Mu, L.L. Kerr, N. Leyarovska, Extended X-ray absorption fine structure study of p-type nitrogen doped ZnO, Chem. Phys. Lett. 469 (2009) 318–320, https://doi.org/10.1016/j.cplett.2009.01.011.

[68] M.W. Kadi, D. McKinney, R.M. Mohamed, I.A. Mkhalid, W. Sigmund, Fluorine doped zinc oxide nanowires: enhanced photocatalysts degrade malachite green dye under visible light conditions, Ceram. Int. 42 (2016) 4672–4678, https://doi.org/10.1016/j.ceramint.2015.11.052.

[69] S.S. Abdullahi, S. Güner, Y. Koseoglu, I.M. Musa, B.I. Adamu, M.I. Abdulhamid, Simple method for the determınatıon of band gap of a nanopowdered sample usıng Kubelka munk theory, Journal of the Nigerian Association of Mathematical Physics 35 (2016) 241–246. https://www.researchgate.net/publication/305810656.

[70] M. Abu Sayed, M. Kamruzzaman, M.A. Sayed, M. Kamruzzaman, The Effects of Dual Acceptor (Na, N) Doping on Zn and O Sites in ZnO, (n.d.).

[71] A.P. Bhirud, S.D. Sathaye, R.P. Waichal, L.K. Nikam, B.B. Kale, An eco-friendly, highly stable and efficient nanostructured p-type N-doped ZnO photocatalyst for environmentally benign solar hydrogen production, Green Chem. 14 (2012) 2790–2798, https://doi.org/10.1039/C2GC35519A.

[72] S.K. Satpathy, U.K. Panigrahi, R. Biswal, P. Mallick, Investigation on the microstructural, optical and magnetic properties of Ce doped ZnO nanorods, Materialia (Oxf). 25 (2022), 101536, https://doi.org/10.1016/j.mtla.2022.101536.

[73] S.K. Satpathy, U.K. Panigrahi, R. Biswal, P. Mallick, Tuning the optical properties of ZnO nanorods through Gd doping, Proceedings of the National Academy of Sciences India Section A - Physical Sciences 93 (2023) 197–204, https://doi.org/10.1007/s40010-022-00798-5.

[74] A. Kumar, S. Mukherjee, H. Sharma, U.K. Dwivedi, S. Kumar, R.K. Gangwar, R.K. Choubey, Role of deposition parameters on the properties of the fabricated heterojunction ZnS/p-Si Schottky diode, Phys. Scripta 97 (2022), 45819, https://doi.org/10.1088/1402-4896/ac6078.

[75] N. Goswami, D.K. Sharma, Structural and optical properties of unannealed and annealed ZnO nanoparticles prepared by a chemical precipitation technique, Physica E Low Dimens Syst Nanostruct 42 (2010) 1675–1682, https://doi.org/10.1016/J.PHYSE.2010.01.023.

[76] A. Boonchun, W.R.L. Lambrecht, Electronic structure of defects and doping in ZnO: oxygen vacancy and nitrogen doping, Phys. Status Solidi 250 (2013) 2091, https://doi.org/10.1002/PSSB.201300010. –2101.

[77] S. Lautenschlaeger, M. Hofmann, S. Eisermann, G. Haas, M. Pinnisch, A. Laufer, B.K. Meyer, A model for acceptor doping in ZnO based on nitrogen pair formation, Phys. Status Solidi 248 (2011) 1217–1221, https://doi.org/10.1002/PSSB.201046516.

[78] S.A. Ayon, M.M. Billah, S.S. Nishat, A. Kabir, Enhanced photocatalytic activity of Ho3+ doped ZnO NPs synthesized by modified sol-gel method: an experimental and theoretical investigation, J. Alloys Compd. 856 (2021), https://doi.org/10.1016/j.jallcom.2020.158217.

[79] R.B.M. Cross, M.M. De Souza, E.M. Sankara Narayanan, A low temperature combination method for the production of ZnO nanowires, Nanotechnology 16 (2005) 2188–2192, https://doi.org/10.1088/0957-4484/16/10/035.

[80] X.L. Wu, G.G. Siu, C.L. Fu, H.C. Ong, Photouminescence and cathodoluminescence studies of stoichiometric and oxygen-deficient ZnO films, Appl. Phys. Lett. 78 (2001) 2285–2287, https://doi.org/10.1063/1.1361288.

[81] J.D. Ye, S.L. Gu, F. Qin, S.M. Zhu, S.M. Liu, X. Zhou, W. Liu, L.Q. Hu, R. Zhang, Y. Shi, Y.D. Zheng, Correlation between green luminescence and morphology evolution of ZnO films, Appl. Phys. Mater. Sci. Process 81 (2005) 759–762, https://doi.org/10.1007/s00339-004-2996-0.

[82] T. Voss, I. Kudyk, L. Wischmeier, J. Gutowski, Nonlinear optics with ZnO nanowires, Phys. Status Solidi B 246 (2009) 311–314, https://doi.org/10.1002/pssb.200880307.

[83] B. Debnath, G. Halder, S. Bhattacharyya, One-step synthesis, structural and optical characterization of self-assembled zno nanoparticle clusters with quench-induced defects, Sci. Adv. Mater. 6 (2014) 1160–1169, https://doi.org/10.1166/sam.2014.1881.

[84] Y. Gong, T. Andelman, G.F. Neumark, S. O'Brien, I.L. Kuskovsky, Origin of defect-related green emission from ZnO nanoparticles: effect of surface modification, Nanoscale Res. Lett. 2 (2007) 297–302, https://doi.org/10.1007/s11671-007-9064-6.

[85] L. Kumar Jangir, Y. Kumari, A. Kumar, M. Kumar, K. Awasthi, Investigation of luminescence and structural properties of ZnO nanoparticles, synthesized with different precursors, Mater. Chem. Front. 1 (2017) 1413–1421, https://doi.org/10.1039/c7qm00058h.

[86] C.H. Ahn, Y.Y. Kim, D.C. Kim, S.K. Mohanta, H.K. Cho, A comparative analysis of deep level emission in ZnO layers deposited by various methods, J. Appl. Phys. 105 (2009) 1–6, https://doi.org/10.1063/1.3054175.

[87] A.B. Djurišić, Y.H. Leung, K.H. Tam, L. Ding, W.K. Ge, H.Y. Chen, S. Gwo, Green, yellow, and orange defect emission from ZnO nanostructures: influence of excitation wavelength, Appl. Phys. Lett. 88 (2006) 28–31, https://doi.org/10.1063/1.2182096.

[88] K.J. Chen, T.H. Fang, F.Y. Hung, L.W. Ji, S.J. Chang, S.J. Young, Y.J. Hsiao, The crystallization and physical properties of Al-doped ZnO nanoparticles, Appl. Surf. Sci. 254 (2008) 5791–5795, https://doi.org/10.1016/j.apsusc.2008.03.080.

[89] J.C. Sin, S.M. Lam, K.T. Lee, A.R. Mohamed, Photocatalytic performance of novel samarium-doped spherical-like ZnO hierarchical nanostructures under visible light irradiation for 2,4-dichlorophenol degradation, J. Colloid Interface Sci. 401 (2013) 40–49, https://doi.org/10.1016/j.jcis.2013.03.043.
[90] Y. Liang, N. Guo, L. Li, R. Li, G. Ji, S. Gan, Preparation of porous 3D Ce-doped ZnO microflowers with enhanced photocatalytic performance, RSC Adv. 5 (2015) 59887–59894, https://doi.org/10.1039/c5ra08519e.
[91] A.R. Khantoul, M. Sebais, B. Rahal, B. Boudine, O. Halimi, Structural and optical properties of zno and co doped ZnO thin films prepared by sol-gel, Acta Phys Pol A 133 (2018) 114–117, https://doi.org/10.12693/APhysPolA.133.114.
[92] A. Kumar, S. Mukherjee, H. Sharma, D.K. Rana, A. Kumar, R. Kumar, R.K. Choubey, Fabrication of low-cost and fast-response visible photodetector based on ZnS:Mn/p-Si heterojunction, Mater. Sci. Semicond. Process. 155 (2023), 107226, https://doi.org/10.1016/j.mssp.2022.107226.
[93] N. Huang, J. Shu, Z. Wang, M. Chen, C. Ren, W. Zhang, One-step pyrolytic synthesis of ZnO nanorods with enhanced photocatalytic activity and high photostability under visible light and UV light irradiation, J. Alloys Compd. 648 (2015) 919–929, https://doi.org/10.1016/j.jallcom.2015.07.039.
[94] Y. Chen, H. Zhao, B. Liu, H. Yang, Charge separation between wurtzite ZnO polar {001} surfaces and their enhanced photocatalytic activity, Appl. Catal., B 163 (2015) 189–197, https://doi.org/10.1016/j.apcatb.2014.07.044.
[95] I.M.P. Silva, G. Byzynski, C. Ribeiro, E. Longo, Different dye degradation mechanisms for ZnO and ZnO doped with N (ZnO:N), J. Mol. Catal. Chem. 417 (2016) 89–100, https://doi.org/10.1016/j.molcata.2016.02.027.
[96] A. Nibret, O.P. Yadav, I. Diaz, A.M. Taddesse, Cr-N co-doped ZnO nanoparticles: synthesis, characterization and photocatalytic activity for degradation of thymol blue, Bull. Chem. Soc. Ethiop. 29 (2015) 247–258, https://doi.org/10.4314/bcse.v29i2.8.
[97] R. Kabir, M.A.K. Saifullah, A.Z. Ahmed, S.M. Masum, M.A.I. Molla, Synthesis of n-doped zno nanocomposites for sunlight photocatalytic degradation of textile dye pollutants, Journal of Composites Science 4 (2020), https://doi.org/10.3390/jcs4020049.
[98] Z. Jia, D. Ren, L. Xu, R. Zhu, Preparation, characterization and photocatalytic activity of porous zinc oxide superstructure, Mater. Sci. Semicond. Process. 3 (2012) 270–276, https://doi.org/10.1016/J.MSSP.2012.02.012.
[99] C. Wu, Facile one-step synthesis of N-doped ZnO micropolyhedrons forefficient photocatalytic degradation of formaldehyde undervisible-light irradiation, Appl. Surf. Sci. 319 (2014) 237–243, https://doi.org/10.1016/j.apsusc.2014.04.217.
[100] J. Zheng, L. Sun, C. Jiao, Q. Shao, J. Lin, D. Pan, N. Naik, Z. Guo, Hydrothermally synthesized Ti/Zr bimetallic MOFs derived N self-doped TiO2/ZrO2 composite catalysts with enhanced photocatalytic degradation of methylene blue, Colloids Surf. A Physicochem. Eng. Asp. 623 (2021), 126629, https://doi.org/10.1016/j.colsurfa.2021.126629.
[101] J.L. Lyons, A. Janotti, C.G. Van De Walle, Why nitrogen cannot lead to p -type conductivity in ZnO, Appl. Phys. Lett. 95 (2009) 1–4, https://doi.org/10.1063/1.3274043.
[102] Y. Qiu, K. Yan, H. Deng, S. Yang, Secondary branching and nitrogen doping of ZnO nanotetrapods: building a highly active network for photoelectrochemical water splitting, Nano Lett. 12 (2012) 407–413, https://doi.org/10.1021/nl2037326.
[103] M.A. Qamar, S. Shahid, M. Javed, M. Sher, S. Iqbal, A. Bahadur, D. Li, Fabricated novel g-C3N4/Mn doped ZnO nanocomposite as highly active photocatalyst for the disinfection of pathogens and degradation of the organic pollutants from wastewater under sunlight radiations, Colloids Surf. A Physicochem. Eng. Asp. 611 (2021), 125863, https://doi.org/10.1016/j.colsurfa.2020.125863.